J Nanopart Res (2016) 18:44
DOI 10.1007/s11051-016-3348-7

RESEARCH PAPER

Suppression of the exaggerated growth of barium ferrite nanoparticles from solution using a partial substitution of Sc^{3+} for Fe^{3+}

Darja Lisjak · Mitja Bukovec · Klementina Zupan

Received: 4 September 2015 / Accepted: 25 January 2016 / Published online: 8 February 2016

Abstract The effect of the substitution of Sc^{3+} for Fe^{3+} in barium ferrite on the size of the resulting nanoparticles was studied. These nanoparticles, with the nominal compositions $BaFe_{12}O_{19}$ and $BaFe_{11.5}Sc_{0.5}O_{19}$, were synthesized hydrothermally at 90–240 °C or by coprecipitation under reflux at 140 °C. The precursors were obtained using (co)precipitation at room temperature. The sizes and morphologies of the precursors and nanoparticles were inspected with transmission electron microscopy, while their structures were confirmed with a combination of X-ray powder and electron diffraction. The samples' compositions were analyzed with energy-dispersive X-ray spectroscopy. The evolution of the particle size and its distribution with the synthesis temperature and time were studied in pure and Sc-substituted barium ferrite and correlated with the evolution of the magnetic properties. The Sc substitution in the barium ferrite results in the formation of magnetic nanoparticles with applicable magnetic properties and in a significant reduction of the exaggerated particle growth. This was explained on the basis of the reaction kinetics.

Keywords Ferrites · Nanoparticles · Particle growth · Magnetic properties

Introduction

Nanoparticles are very interesting because their small size has significant effects on their physical properties. However, in order to study and exploit these effects, the nanoparticles should be in a specific size range. Therefore, the synthesis of nanoparticles with controlled sizes and functional physical properties is of prime importance. Nanoparticles are usually produced by wet-chemical synthesis. The crystallization of the particles from solutions can be divided into three stages: nucleation, primary growth, and secondary growth (Jolivet 2000). In general, a homogeneous particle size can be obtained if the nucleation and growth stages are separated. Consequently, the secondary growth due to Ostwald ripening is suppressed. Namely, Ostwald ripening is a consequence of a continuous precipitation and dissolution and is favored in systems with inhomogeneous particle sizes (Jolivet 2000; Fuerdi-Milhofer 1981). Most often, the size of nanoparticles is controlled by specific capping agents that are introduced during the synthesis and coordinate

Electronic supplementary material The online version of this article (doi:10.1007/s11051-016-3348-7) contains supplementary material, which is available to authorized users.

D. Lisjak (✉) · M. Bukovec
Department for Materials Synthesis, Jožef Stefan Institute, Ljubljana, Slovenia
e-mail: darja.lisjak@ijs.si

K. Zupan
Faculty for Chemistry and Chemical Technology, University of Ljubljana, Ljubljana, Slovenia

with the nanoparticle surfaces (Tian et al. 2003; Moon et al. 2009; Primc et al. 2009). At the same time, the selected capping agent also provides the colloidal stability of the nanoparticles in a specific solvent. However, in some cases, the size-control capping agents are not suitable for the specific final applications of nanoparticles. In such cases, the capping agent should be replaced by, for example, a ligand-exchange process (Dong et al. 2011), with another capping agent. This step substantially decreases the synthesis yield, which is a constant problem with nanoparticles. An alternative possibility for controlling the nanoparticle size is chemical substitution (or doping). The variation of the lanthanide (Ln^{3+}) ions in different fluorides affected the size, structure, and/or morphology of fluorescent fluoride ($NaLnF_4$) nanoparticles (Li et al. 2008; Wang et al. 2010). Similarly, the particle size distribution was significantly narrowed by the partial substitution of Fe^{3+} in barium ferrite ($BaFe_{12}O_{19}$) with larger cations (i.e., In^{3+} or Sc^{3+}) (Lisjak and Drofenik 2012).

Barium ferrite is a hexagonal ferrite with large magnetocrystalline anisotropy. Its crystals assume a hexagonal, plate-like habit with a magnetoplumbite structure. Barium ferrite possesses uniaxial magnetic anisotropy and its magnetic easy axis is parallel to the crystallographic *c*-axis. It has been traditionally used in hard-magnetic, magnetic recording, and high-frequency applications (Pullar 2012). Recently, it was applied in multifunctional (nano)composites for magnetic photocatalysis, magneto-optics, magneto-electrics, and magnetic gels (Lee et al. 2006; Srnivas et al. 2009; Mertelj et al. 2013; Ferk et al. 2015; Mitsumata et al. 2008). The preparation of composites requires a homogeneous distribution of the functional particles (with no agglomeration) in the matrix. This is a challenging task in the case of magnetic particles that tend to agglomerate due to the magnetic dipole attraction. Although this magnetic dipole attraction energy can be reduced by decreasing the particle size to a few nanometers, this decrease should be optimized with respect to the magnetic properties, which also deteriorate with the decreasing size of nanoparticles (Kodama 1999).

Barium ferrite nanoparticles can be synthesized hydrothermally at a minimum of 80 °C or with coprecipitation using reflux at a minimum of 90 °C (Che et al. 2003; Drofenik et al. 2010; Matijević 1987; Sada et al. 1991). The low-temperature formation of barium ferrite is a homogeneous phase reaction and its mechanism is based on several reaction steps (Wang and Shih 1991):

$$x\mathrm{Fe(OH)_4^-(aq)} \leftrightarrow \left[\mathrm{Fe(OH)_4}\right]_x^{-x}(\mathrm{aq}), \quad \text{where } 0 < x < 12, \tag{1a}$$

$$\left[\mathrm{Fe(OH)_4}\right]_x^{x-}(\mathrm{aq}) + \mathrm{Ba(aq)^{2+}} \leftrightarrow \mathrm{BaO \cdot Fe_2O_3 \cdot}\left[\mathrm{Fe(OH)_4}\right]_y^{-y}(\mathrm{aq}), \quad \text{where } y = x - 2, \tag{1b}$$

$$\left[\mathrm{Fe(OH)_4}\right]_z^{-z}(\mathrm{aq}) + \mathrm{BaO \cdot Fe_2O_3 \cdot}\left[\mathrm{Fe(OH)_4}\right]_y^{-y}(\mathrm{aq}) \leftrightarrow \mathrm{BaFe_{12}O_{19}(s) + 15 \cdot H_2O(l) + 10 \cdot OH^-(aq)}, \quad \text{where } y + z = 10. \tag{1c}$$

The *x* value depends on the concentration of OH^-. The formation of an intermediate (Eq. 1b) increases the reaction rate in comparison with the potential direct formation of $BaFe_{12}O_{19}$ from 1 mol of Ba^{2+} and 12 mol of $FeOH_4^-$. The insoluble $BaFe_{12}O_{19}$ shifts the chemical equilibrium to the right-hand side. The newly formed OH^- ions increase the concentration of $\left[\mathrm{Fe(OH)_4}\right]_x^{x-}$ to supersaturation and enable the nucleation and crystallization of $BaFe_{12}O_{19}$ at moderate temperatures (Drofenik et al. 2007). This is important since at high enough temperatures (≥120 °C), barium ferrite nanoparticles with a bimodal size distribution are formed as a consequence secondary growth based on Ostwald ripening. These nanoparticles consist of discoid 10-nm particles and nanoplates with diameters up to a few hundred nanometers, and having thicknesses of a few nanometers. However, only small discoid barium ferrite nanoparticles are formed below 120 °C. They are superparamagnetic at room temperature and have a saturation magnetization (M_s) of a few emu/g (Drofenik et al. 2010), which is not suitable for any potential application. Barium ferrite nanoparticles of comparable size, morphology, and magnetic properties can be synthesized hydrothermally with the addition of oleic acid at as high as 160 °C (Primc et al. 2009). As mentioned above, barium ferrite nanoplates with diameters of around 50–100 nm and an M_s of around 30 emu/g can be synthesized hydrothermally at 240 °C when the Fe^{3+} is partly substituted with Sc^{3+}. These barium ferrite nanoplates are dispersible in various alcohols and show a magneto-optical response when incorporated

into polymers or liquid crystals (Mertelj et al. 2013; Ferk et al. 2015). The aim of this work was to compare the kinetics for the growth of the pure barium ferrite ($BaFe_{12}O_{19}$) and the Sc-substituted barium ferrite ($BaSc_{0.5}Fe_{11.5}O_{19}$) nanoparticles from solution in order to be able to tune the particle size (distribution) with respect to their final application.

Methods

Synthesis

Barium, scandium and iron nitrates, and NaOH were purchased from Alfa Aesar. HNO_3 was purchased from Carlo Erba Reagents S.A.S. All the chemicals were used without any further purification. The precise metal concentration in the nitrates was determined using optical emission spectroscopy with inductively coupled plasma (Agilent 720).

Nanoparticles with compositions of $BaFe_{12}O_{19}$ (BF) and $BaSc_{0.5}Fe_{11.5}O_{19}$ (Sc05) were synthesized from aqueous solutions of nitrates with a molar ratio of Ba:Fe = 1:5 and Ba:Fe:Sc = 1:4.5:0.5, respectively. The required surplus of Ba with respect to the nominal composition was determined previously (Drofenik et al. 2007). NaOH [molar ratio of (OH):(Ba + Fe + Sc) >10] was used as a precipitating agent. The slurry was transferred to an Inconel autoclave (Parr Instruments) and was heated to 90–240 °C for 0–24 h. The autoclave was naturally cooled to room temperature. The as-synthesized particles were washed with water and HNO_3 to dissolve the $BaCO_3$ (side product) and were kept in a water suspension until they were analyzed.

In a similar way, the samples were also prepared under reflux. In this case, the coprecipitated slurry was transferred to a Teflon beaker, closed with a cooling unit that enabled the reflux of the evaporated water. The slurry was heated to 90–140 °C for 0–24 h. The particles were washed as described above. The samples synthesized hydrothermally and under reflux were labeled as HT and R, respectively.

For the precursor studies, the (co)precipitates from different cations (Ba–Fe and Ba–Fe–Sc) were obtained as above or using a stoichiometric ratio of Ba:Fe, as in the nominal compositions ($BaFe_{12}O_{19}$ and $BaSc_{0.5}Fe_{11.5}O_{19}$). Here we evaluated only a potential effect of the Ba:Fe ratio on the formation of precursors, while this effect on the formation of BF was reported previously (Drofenik et al. 2007).

For a comparison, cobalt ferrite nanoparticles with a spinel structure and the nominal compositions $CoFe_2O_4$ (labeled as CF) and $CoFe_{1.9}Sc_{0.1}O_4$ (labeled as CF-Sc01) were synthesized hydrothermally at 120 and 200 °C with a holding time of 2 h. Details of the synthesis can be found in Jenuš and Lisjak (2014).

Characterization

The magnetic properties of the dried nanoparticles were measured with a vibrating-sample magnetometer (VSM, LakeShore 7404). The particle morphologies and sizes were evaluated with a transmission electron microscope (TEM, Jeol 2100) equipped with an energy-dispersive X-ray spectrometer (EDXS) for the chemical microanalysis. The equivalent diameters of the particles were determined from their surfaces using digital micrograph software (Gatan, Inc.). A minimum of 150 particles per sample was counted for the statistics. The particles' thicknesses were directly determined from the TEM images. The samples were also analyzed with X-ray powder diffraction using Cu Kα radiation (XRD, Siemens D5000). The XRD analysis was performed with Topas software (Bruker, AXS) using the Pawley method (1981).

Results

Precursors

In the first step of a hydrothermal synthesis, the precursors are formed by a coprecipitation of the dissolved cations, in our case from Ba^{2+}, Fe^{3+}, (and Sc^{3+}). This happens at room temperature prior to the formation of the barium ferrite. The XRD analyses revealed witherite ($BaCO_3$) as the only crystalline phase in the precursors (Fig. 1). This must have originated from the excess of barium nitrate in the starting composition (see "Synthesis" section: atomic ratio Ba:Fe = 1:5 and Ba:Fe:Sc = 1.0:4.5:0.5). Namely, the Ba–Fe and Ba–Fe–Sc precursors with a stoichiometric ratio of cations (atomic ratio Ba:Fe = 1:12 and Ba:Fe:Sc = 1.0:11.5:0.5, respectively) were amorphous. In general, no difference was observed between the Ba–Fe and the Ba–Fe–Sc precursors.

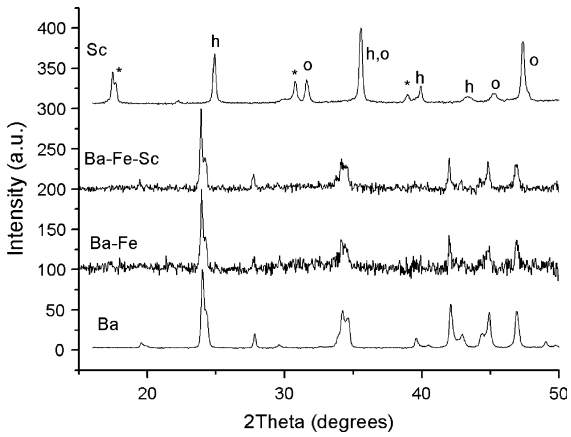

Fig. 1 XRD diffractograms of (co)precipitates of denoted cations. The *peaks* marked with *o* and *h* correspond to Sc_2O_3 (μPDSM no. 23-1402) and ScOOH (μPDSM no. 20-1035), respectively. Unidentified *peaks* are marked with *asterisk*. All the other *peaks* correspond to $BaCO_3$ (μPDSM no. 45-1471)

TEM observations concurred with the XRD data. The precursors were composed of an amorphous network in which crystalline angular nanoparticles with sizes of around 100 nm were embedded. As an example, see Fig. S1 in Online Resource. The SAED pattern of the large nanoparticles corresponded to $BaCO_3$. This was also consistent with the EDXS analysis, where only Ba was detected in the larger nanoparticles, while Ba, Fe (and Sc) were detected in the amorphous phase. No evidence of any crystalline phase, not even for the $BaCO_3$, was found in the stoichiometric precursors of Ba–Fe and Ba–Fe–Sc. All these suggest that the presence of Fe^{3+} inhibits the crystallization of the $BaCO_3$ and Sc compounds. Note that the pure Ba and Sc coprecipitates were crystalline (Fig. 1). In this step, we did not find any evidence that Sc substitution would affect the formation of the precursor(s).

Barium ferrite precursors are amorphous coprecipitates of all the constituent cations and can precipitate as homogeneous mixtures of (oxy)hydroxides or from an intermediate phase (Eq. 1b). The coprecipitation takes place at room temperature, which is too low for the formation of $BaFe_{12}O_{19}$ (Eq. 1c). However, the precursors dissolve in a highly basic environment at an elevated temperature allowing for all the reactions steps in Eqs. 1a–1c to take place. The $BaCO_3$, which crystallizes from the surplus of Ba^{2+}, is a very stable compound with a negligible solubility under the reaction conditions and is necessary to prevent the crystallization of other Ba–Fe compounds, i.e., $BaFe_{4}O_{7}$ (Drofenik et al. 2007). The $BaCO_3$ does not affect the formation mechanism of the $BaFe_{12}O_{19}$ and has to be dissolved during the purification of the as-synthesized nanoparticles (see "Synthesis" section).

Primary particle growth

The crystallization of barium ferrite nanoparticles at the studied temperatures (≥90 °C) was fast and, consequently, it was not possible to identify the nucleation stage. No evidence of a residual amorphous phase was found in any of our samples, not even for the 0-h synthesis time. This is consistent with the previously reported formation of barium ferrite at as low as 80 or 90 °C (HT or R synthesis, respectively) (Drofenik et al. 2010). At these temperatures, the nuclei of barium ferrite are in equilibrium with the dissolved species from Eq. 1 [including $Sc(OH)_4^-$] (Baes and Mesmer 1976; Drofenik et al. 2007; Wang and Shih 1991) and the primary barium ferrite particles crystallize from nuclei via a dissolution–recrystallization process. Similar to this, the secondary growth proceeds at higher synthesis temperatures (or longer synthesis times). Primary and secondary particles were distinguished with respect to their size, shape, and magnetic properties (Tables 1; S1 in Online Resource).

Primary barium ferrite particles are very fine nanoparticles of irregular shape. Their crystal structure deviates from that of the bulk (Makovec et al. 2012) and they are superparamagnetic at room temperature (for more details on magnetic properties, see "Magnetic properties" section). As an example, we show the TEM images of the HT-Sc05 nanoparticles synthesized at 90 °C for 0 h (Fig. 2). Most of the nanoparticles appeared to be of quasi-spherical shape, with diameters of around 10 nm or less. Although most of the particles lay flat on a TEM supporting grid, a few of them were positioned perpendicularly (see the encircled particles in Fig. 2a, b). A thorough inspection of many sample batches and TEM images revealed a few particles per sample with a distinct plate-like shape. From these particles, their thickness was estimated to be 2–3 nm. The SAED pattern shows a diffuse ring pattern, typical for nanocrystallites. The indices correspond to the hexagonal space group $P6_3/mmc$ (194) of $BaFe_{12}O_{19}$ and are in agreement with the XRD data (Fig. S2 in Online Resource). In contrast to this, a few

Table 1 Synthesis conditions of the specific growth stages for barium ferrite nanoparticles

Samples	Primary growth	Secondary growth	
		Moderate growth	Exaggerated growth
HT-BF	$T = 90$ °C, $t < 6$ h	$T = 90$ °C, $t \geq 6$ h	$T = 90$ °C, $t = 21$ h
		$T \geq 110$ °C, $t = 0$ h	$T \geq 140$ °C, $t = 0$ h
HT-Sc05	$T = 90$ °C, $t = 0$ h	$T = 90$ °C, $t \geq 2$ h	$T = 240$ °C, $t = 12$ h
		$T \geq 110$ °C, $t = 0$ h	
R-BF	$T = 140$ °C, $t \leq 12$ h	$T = 140$ °C, $t > 12$ h	–
R-Sc05	$T = 140$ °C, $t \leq 12$ h	$T = 140$ °C, $t > 12$ h	–

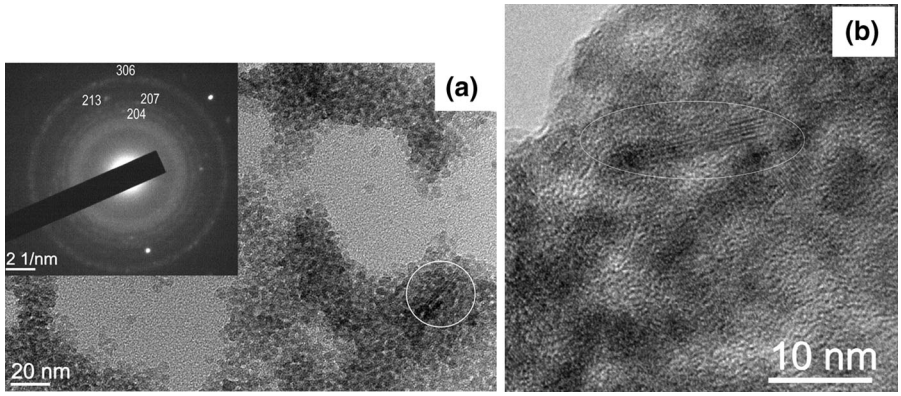

Fig. 2 TEM images of the HT-Sc05 sample synthesized at 90 °C for 0 h with the corresponding SAED pattern (**a**) and an image at higher resolution (**b**). The two particles lying perpendicular to the TEM grid are *encircled* (**a**, **b**). The *indices* (**a**) correspond to the $BaFe_{12}O_{19}$ structure (space group $P6_3/mmc$)

very bright dots in the SAED pattern suggest that some of the nanocrystallites are larger and of better crystallinity than the average, for example, the encircled particles in Fig. 2. The EDXS analysis confirmed that the particles were composed of Ba, Fe, Sc, and O. The situation was similar for the HT-BF nanoparticles synthesized at 90 °C for 0 h and the R nanoparticles of both compositions synthesized at 140 °C for 0 h.

Secondary and exaggerated particle growth

The secondary particles were distinguished from the primary particles by their distinct plate-like shape. The number and size of the plate-like particles, for both compositions, increased with the synthesis time (Figs. 3; S3 in Online Resource). Larger particles with a broader size distribution were obtained in the pure BF samples than in those with the Sc05 composition. This difference increased with the synthesis time. Note that all constituting elements (Ba, Fe, O, and Sc in the case of Sc05 compositions) were identified with EDXS for all the samples.

The particle growth was faster at higher synthesis temperatures (0-h synthesis time) and increased significantly, together with the size distribution, above 140 °C (Fig. 4a–c; Table S1 in Online Resource). The Sc substitution decreases the particle size and its distribution, and this effect becomes more significant with the increasing synthesis temperature. As an example we show TEM images of the HT samples synthesized at 200 °C for 0 h (Fig. 4d, e). While only plate-like particles with a much more homogeneous size can be seen in the HT-Sc05 sample, fine nanoparticles of around 10 nm (as an example, see encircled nanoparticles in Fig. 4e) can be seen together with the plate-like nanoparticles with diameters up to several hundreds of nanometers in the HT-BF sample.

We can distinguish the moderate versus exaggerated particle growth from the ratio of the maximum versus the average particle size (Rat) and/or the difference between the maximum and the minimum particle size (Dif) (Fig. 5). Both inhomogeneity parameters increase significantly for the HT-BF

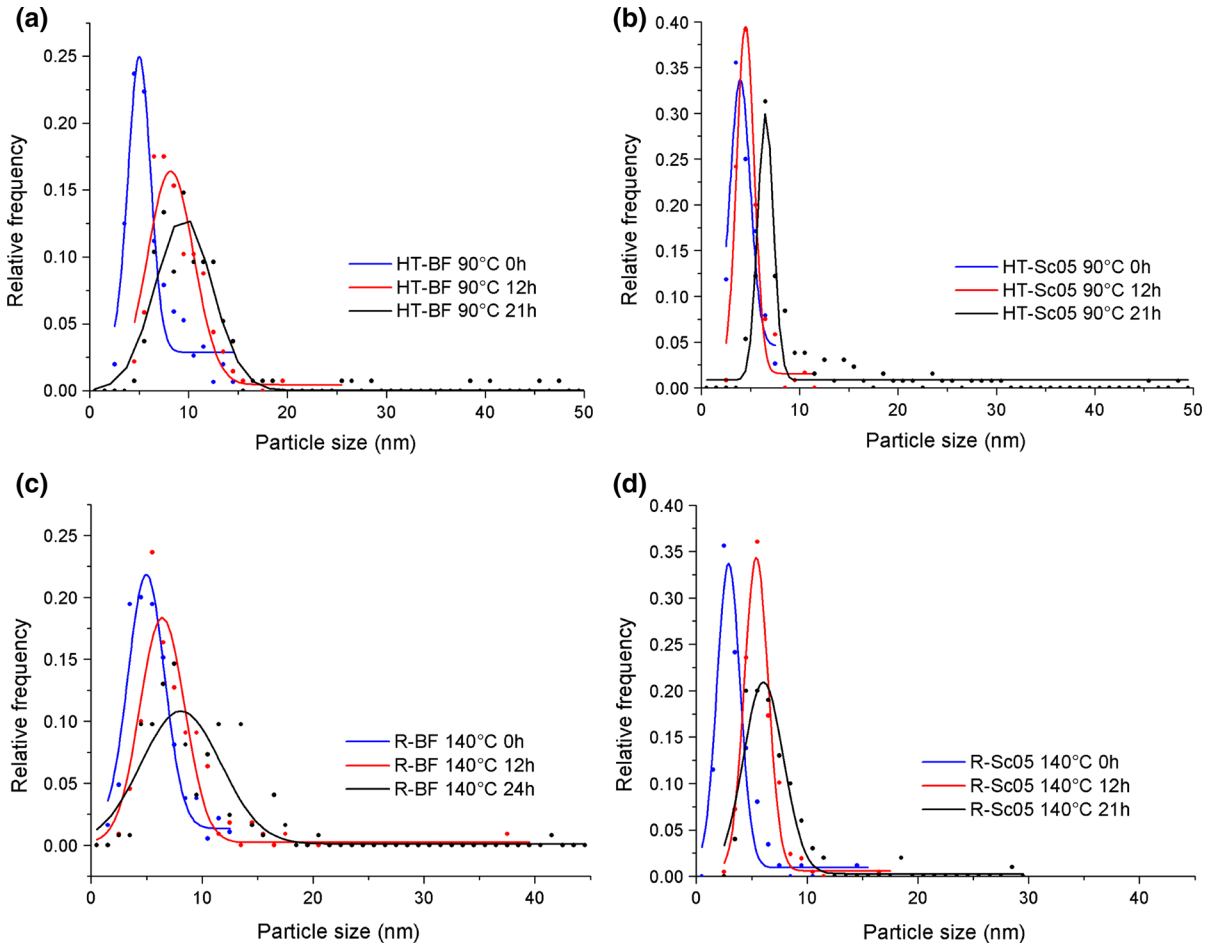

Fig. 3 Particle size distribution of the HT (**a**, **b**) and R (**c**, **d**) samples synthesized at 90 and 140 °C, respectively, with different synthesis times: BF (**a**, **c**) and Sc05 (**b**, **d**)

samples synthesized at temperatures of 140 °C or higher, while much smaller values for both parameters are observed for the HT-Sc05 samples (Fig. 5a). This suggests that exaggerated particle growth in the pure HT-BF samples starts at 140 °C, while it was suppressed in the HT-Sc05 samples.

To exclude the exaggerated growth from the analysis, we evaluated the effect of the synthesis time on the HT samples at 90 °C (Fig. 5b). A small increase in the particle size inhomogeneity is observed for the 21-h synthesis time. Both inhomogeneity parameters are larger and vary more significantly for the HT-BF than for the HT-Sc05 nanoparticles and suggest the possible onset of exaggerated particle growth in the HT-BF at 90 °C after 21 h. We can conclude that the exaggerated growth of the HT-BF particles begins under much milder synthesis temperatures and is faster than that of the HT-Sc05 particles (Table 1). Although the exaggerated particle growth in the R samples can be neglected, we can see that the inhomogeneity parameters (Fig. 5c) are also larger and increase with the synthesis time more significantly for the R-BF than for the R-Sc05 samples.

Magnetic properties

The saturation magnetization (M_s) and coercivity (H_c) values increase with the synthesis temperature and time up to 35 emu/g and over 1000 Oe, respectively (Fig. 6). These values are lower than those of the bulk ($M_s \sim 60$–70 emu/g, $H_c = 3000$–4000 Oe) (Pullar 2012). This is an indication of a small nanoparticle size and/or a poor crystalline order, which both increase/improve with the synthesis temperature. In

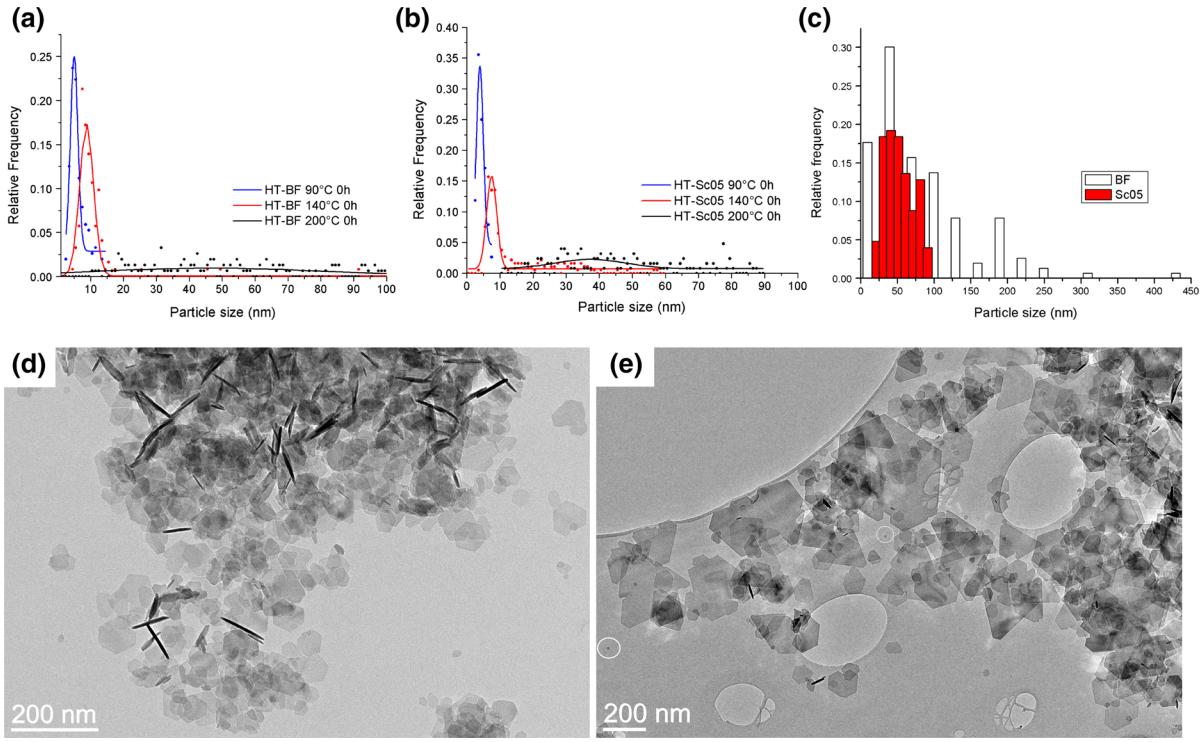

Fig. 4 Particle size distribution of the HT samples synthesized at different synthesis temperatures with a 0-h synthesis time: HT-BF (**a**) and HT-Sc05 (**b**). Particle size distribution in **c** corresponds to the samples synthesized at 200 °C shown in TEM images: HT-Sc05 (**d**) and HT-BF (**e**). The particle size *axis* (**a**, **b**) was limited for the sake of clarity; see Table S1 in Online Resource for the maximum particle sizes

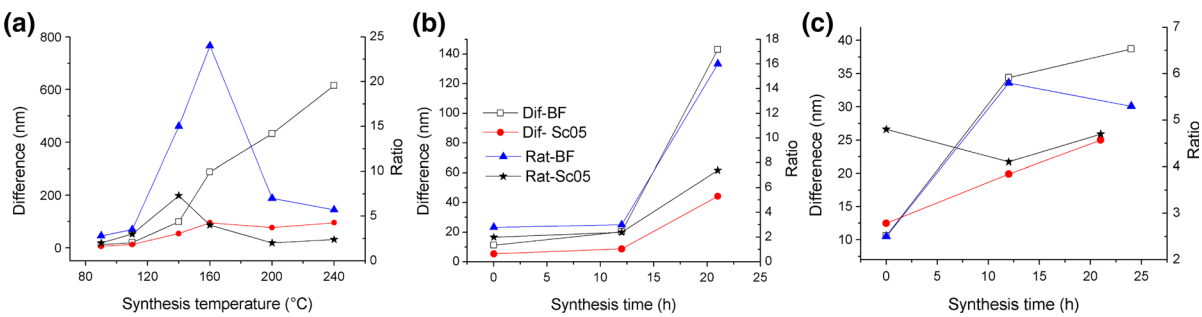

Fig. 5 Variation of the particles size difference (Dif) and ratio (Rat) with the chemical composition and synthesis conditions: HT synthesis at different temperatures with 0-h synthesis time (**a**), HT synthesis at 90 °C with different synthesis times (**b**) and R synthesis at 140 °C with different synthesis times (**c**). *Legend* in **b** also corresponds to **a** and **c**

fact, the HT samples synthesized up to 110 °C show magnetic curves(almost) without hysteresis, similar to superparamagnetic materials ($H_c = 0$ Oe). The R samples show magnetic properties (Table S1 in Online Resource) comparable with those of the HT samples synthesized at 90 °C. In contrast to this, the HT samples synthesized at a minimum of 140 °C are ferrimagnetic and show a magnetic hysteresis ($H_c > 0$ Oe) typical for ferrimagnetic materials. The evolution of the ferrimagnetic behavior coincides with the formation of secondary particles with a plate-like shape, while the primary, quasi-spherical particles are superparamagnetic. The M_s values (Fig. 6a, b) are higher for the HT-Sc05 than for the HT-BF samples up

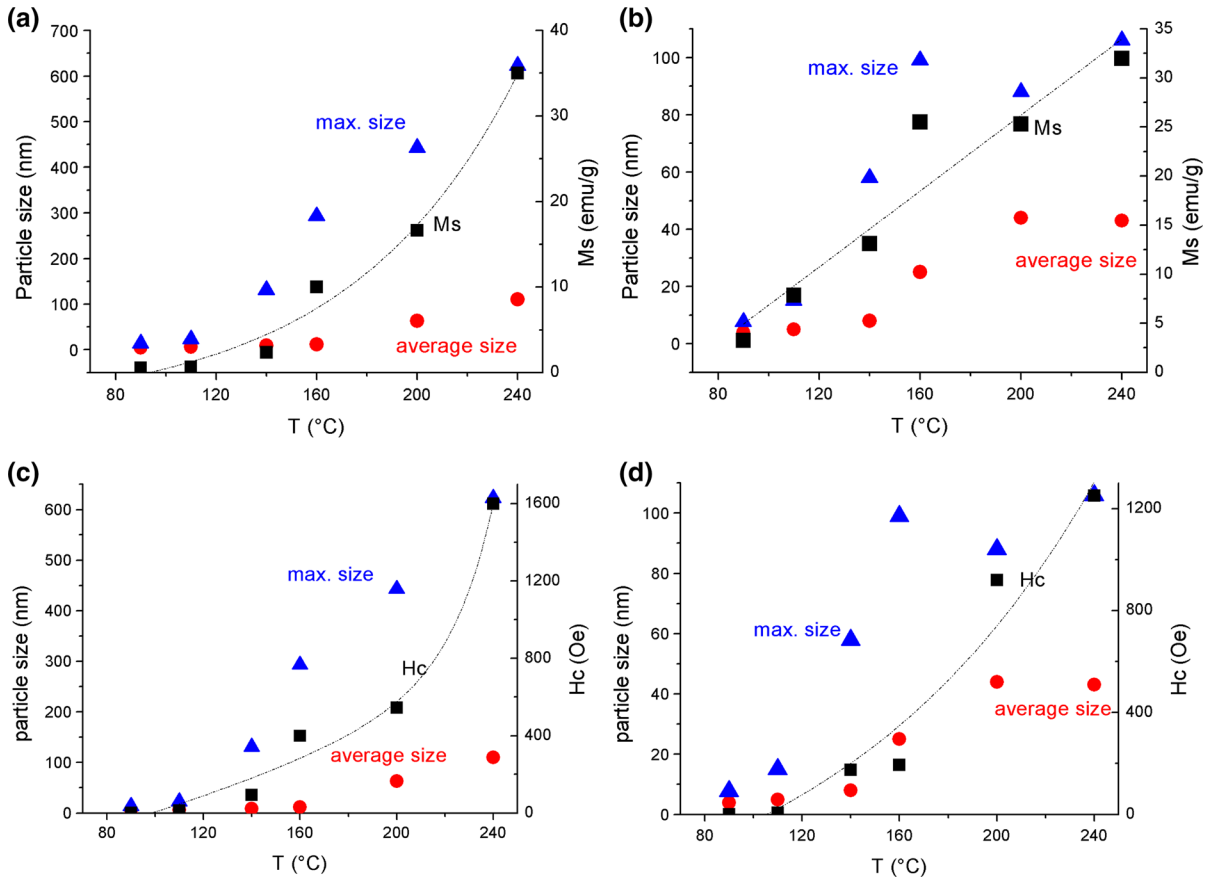

Fig. 6 The effect of the HT synthesis temperature for a 0-h synthesis time on the average and maximum particle size, and the saturation magnetization of the HT-BF (**a**) and HT-Sc05 (**b**) samples, and the coercivity of HT-BF (**c**) and HT-Sc05 (**d**). *Lines* present fitting curves [exponential (**a**, **c**, **d**) and linear (**b**) fit] for a clearer presentation of the variation of the M_s and H_c values with the temperature

to a synthesis temperature of 200 °C, and they also increase faster with the synthesis temperature for the HT-Sc05 than for the HT-BF. In contrast to the M_s values, no significant difference in the H_c values (Fig. 6c, d) could be observed for the two different compositions. They both increase with the synthesis temperature, i.e., with the particle size, as would also be expected for single-domain nanoparticles (Kodama 1999).

The evolution of the magnetic properties of the barium ferrite nanoparticles can be correlated to the particle growth (Fig. 6). While a monotonous (almost linear) increase in the M_s values of the HT-Sc05 samples with an increasing synthesis temperature was observed, the M_s values of the HT-BF samples showed no significant increase up to the synthesis temperature of 140 °C, which was followed by a significant increase in the M_s values above 140 °C. Figure 6 also shows that the evolution of M_s matches better to the increasing maximum size of the nanoparticles than to their average size. The M_s values of the BF and Sc05 nanoparticles varied with the synthesis time in a similar way as with the temperature, correlated with the maximum size of the nanoparticles (Table S1 in Online Resource). This can be explained in terms of the size dependence of the M_s of the nanoparticles, meaning that the contribution of the larger particles to the overall M_s of the samples is significant in comparison to the small particles with negligible M_s values and small masses. Namely, the M_s values are given as the mass magnetization of the samples and they increase with the increasing number of magnetic nanoparticles and with their size (and magnetocrystalline order). The same correlation with the maximum

particle size can also be observed for the H_c values (Fig. 6c, d).

Despite the slower particle growth, the M_s values of the Sc05 nanoparticles increase faster with the synthesis time and temperature than those of the BF nanoparticles (Figs. 6a, b; S4; Table S1 in Online Resource). Another contradiction to the observed is the fact that the Sc^{3+} substitution for Fe^{3+} in bulk barium hexaferrite results in lower M_s values (Röschmann et al. 1984). This can be attributed to the different site occupancies of the cations in the nanocrystals in comparison to the bulk (Makovec et al. 2011). A similar explanation could also be valid in this particular case. Another possible explanation could be related to the thickness of a magnetic dead layer. We showed that the bulk-like crystal order in the barium ferrite nanoplates is limited to a few nm in the interior of the larger nanoplates (sample HT-BF 240 °C 0 h), while the surface layers also deviate from the bulk with respect to the chemical composition (Lisjak et al. 2014). This defect surface layer, i.e., magnetic dead layer, results in inferior magnetic properties when compared to bulk barium ferrite. The greater stability (see "Discussion" section) of the Sc05 nanoparticles versus the BF may also have resulted in a thinner magnetic dead layer and, consequently, in the unexpectedly higher M_s values.

Discussion

Very fine barium ferrite nanoparticles with a quasi-spherical shape were formed at the lowest applied temperatures. While we can assume that these fine nanoparticles are a result of the primary growth, larger plate-like nanoparticles form during the secondary growth via the dissolution of primary particles. Regardless of the synthesis conditions, the size and size distribution of the BF particles are larger than those of the Sc05 particles (see "Results" section) and this difference increases with the synthesis time and temperature (Fig. 5).

Let us first focus on the particle size. We can compare the effect of the substitution of Fe^{3+} with the larger Sc^{3+} to the $NaLnF_4$ system, where the size of the nanoparticles decreased with the size of the Ln^{3+} (Wang et al. 2010). However, the increasing size of the Ln^{3+} coincided with an increasing polarizability, which slowed down the accretion of fresh Ln^{3+} on the nuclei and the particles. In our case, the smaller Fe^{3+} is more polarizable than Sc^{3+} and a different explanation should be applied. The reaction kinetics can be slowed down due to the lower probability for the formation of an intermediate and a stable nucleus (Eqs. 1b, 1c) from three cations than from two cations. Consequently, the nucleation and growth of the Sc05 particles are slower than that of the BF particles. However, the slower particle growth due to the addition of a third cation does not explain the fact that the Cr substitution had no effect on the particle size of the barium ferrite (Lisjak and Drofenik 2012). The main difference between the Cr^{3+} and the Sc^{3+} is their size. While Cr^{3+} is comparable in size to that of Fe^{3+}, the Sc^{3+} is larger. If $Sc(OH)_4^-$ combines with $[Fe(OH)_4]_x^{x-}$ into a larger complex, it can slow down the reaction kinetics and, with it, affect the particle growth. This is consistent with a similar effect involving In substitution (Lisjak and Drofenik 2012). In^{3+} is also larger than Fe^{3+}. Parallel experiments investigating the effect of Sc substitution on the size of cobalt ferrite particles (samples CF and CF-Sc01: see "Synthesis" section) were also in accordance with the above. Note that the coprecipitation of precursors and the synthesis of cobalt ferrite proceeded in the presence of a large excess of the OH^- ions, as was the case for the barium ferrite. Therefore, large Fe complexes (as in Eq. 1a) could also be formed in a combination Fe–Co(–Sc). Smaller particles of cobalt ferrite were synthesized in the Sc-substituted sample (Fig. S5 in Online Resource); however, their particle size distribution was less homogeneous, especially at higher synthesis temperatures. The increase in the synthesis temperature from 120 to 200 °C resulted in the growth of the CF particles from an average size of 12 to 19 nm (approximately 58 %), with an obvious decrease in the fraction of the particles smaller than 10 nm. Under the same conditions, the CF-Sc01 particles' size only increased from an average size of 8 to 11 nm (approximately 38 %) with a large fraction of small particles (<10 nm) at both synthesis temperatures. This was also reflected in the inhomogeneity parameters (Table S2 in Online Resource). The inhomogeneity of the Sc-substituted cobalt ferrite increased with the synthesis temperature, when compared to the pure CF samples. This was just the opposite to the effect of the Sc substitution in barium ferrite. Obviously, only the normal growth of

the CF-Sc01 particles was slowed down due to the presence of an additional cation, but the exaggerated growth was not suppressed. Therefore, the question remaining unanswered is why the particle size is more homogeneous in the Sc05 than in the BF samples (Fig. 5).

First, it must be pointed out that the reaction mechanism itself promotes inhomogeneous particle growth. The formation of a precursor is faster than the nucleation of barium ferrite, since the precursor forms already at room temperature, while the nucleation of barium ferrite was not observed at room temperature, not even after several days. At elevated temperatures, a large excess of OH^- provides a continuous supersaturation with $[Fe(OH)_4]_x^{x-}$ and a continuous nucleation of fresh barium ferrite (Eq. 1), while at the same time enabling a continuous release of fresh OH^-. The nucleation can be homogeneous and heterogeneous—on the firstly formed nuclei (and particles) thus allowing nuclei and particles to form and grow continuously. This inevitably results in a size inhomogeneity and, after a prolonged synthesis time or at a high enough temperature, in exaggerated particle growth (Fig. 4; Table 1). The secondary growth by Ostwald ripening occurs in systems with inhomogeneous particle sizes (Jolivet 2000; Fuerdi-Milhofer 1981). Here, the smaller, less stable particles dissolve faster than the larger particles, which grow continuously at the expense of the smaller particles. Due to the relatively low solubility of BF, its dissolution, and with it the exaggerated growth, becomes significant only at elevated temperatures, i.e., above 140 °C under hydrothermal conditions (Fig. 5a). However, in the presence of Sc^{3+}, the continuous supersaturation with $[Fe(OH)_4]_x^{x-}$ must have been prevented (or suppressed) and the continuous homogeneous nucleation was limited. Namely, a higher supersaturation is required for the homogeneous than for the heterogeneous nucleation (Jolivet 2000; Fuerdi-Milhofer 1981). Consequently, the sizes (and their increase with the synthesis time and temperature) of the Sc05 particles were more homogeneous than that of the BF (Figs. 3a, b, 5b, c; S3 in Online Resource). Additional HT synthesis at high temperature of 240 °C with synthesis time of 12 h resulted in the onset of exaggerated growth also in the Sc05 sample (Fig. S6 in Online Resource). Nevertheless, the size of the plates was much more homogeneous than in the BF sample, in which some of the plates were of submicron size (Fig. 6Sb in Online Resource). Therefore, it can be assumed that the solubility rate of Sc05 nanoparticles at a given synthesis conditions is lower than that of the BF, which contributes to the suppression of the exaggerated growth in Sc05. Moreover, the lower solubility (rate) of Sc05 may also be correlated to its superior magnetocrystalline order, which is implied by the superior magnetic properties (see Fig. 6 and explanation in "Magnetic properties" section). A similar effect on the growth and magnetic properties of the barium ferrite nanoparticles was observed for In substitution (Lisjak and Drofenik 2012), while the opposite effect of the Sc substitution on the magnetic properties was measured in the cobalt ferrite samples (Table S2 in Online Resource). The M_s values of the cobalt ferrite decreased with the Sc substitution, together with the particle size.

All the above suggest that the exaggerated particle growth from a solution can be suppressed by the substitution of larger Sc^{3+} (or In^{3+}) for Fe^{3+} only in combination with Ba^{2+}, i.e., in the case of barium ferrite, and is not effective for the ferrites (i.e., spinel ferrites) in general. This may be correlated with the much larger solubility (rate) of spinel ferrites in comparison with that of barium ferrite.

Conclusions

The effect of substituting Sc^{3+} for Fe^{3+} in barium ferrite on the growth of nanoparticles from solution was studied. The size of the pure barium ferrite nanoparticles was larger and the size distribution was broader than that of the Sc-substituted nanoparticles and the difference increased with the synthesis temperature and time. Moreover, the Sc substitution efficiently suppressed the exaggerated growth of the barium ferrite nanoparticles from solution. This was explained with the slower reaction kinetics and the suppression of the continuous supersaturation due to the lower solubility rate of the particles containing Sc^{3+}. The later was also in accordance with the superior magnetic properties of the Sc-substituted barium ferrite nanoparticles, which makes them interesting for multiferroic and magneto-optical applications. This study also explains the similar effects of In substitution on the growth and magnetic properties of barium ferrite nanoparticles. Finally, the substitution

of Fe^{3+} with larger trivalent cations (like Sc^{3+} or In^{3+}) does not suppress the exaggerated particle growth of ferrite nanoparticles from solution, in general, but it is effective specifically in the case of hexagonal barium ferrites.

Acknowledgments The work was financially supported by Slovenian Research Agency within the Research Program P2-0089 and in part within P1-0175-103. The authors acknowledge the use of equipment at the Center of Excellence in Nanosciences and Nanotechnology. Dr. Sašo Gyergyek is acknowledged for his helpful discussion.

References

Baes CF Jr, Mesmer RE (1976) The hydrolysis of cations. Wiley, New York

Che S, Wang J, Chen Q (2003) Soft magnetic nanoparticles of $BaFe_{12}O_{19}$ fabricated under mild conditions. J Phys Condens Matter 15:L335–L339

Dong A, Ye X, Chen J, Kang Y, Gordon T, Kikkawa JM, Murray CB (2011) A generalized ligand-exchange strategy enabling sequential surface functionalization of colloidal nanocrystals. J Am Chem Soc 133:998–1006

Drofenik M, Kristl M, Žnidaršič A, Hanžel D, Lisjak D (2007) Hydrothermal synthesis of Ba-hexaferrite nanoparticles. J Am Ceram Soc 90:2057–2061

Drofenik M, Ban I, Ferk G, Makovec D, Žnidaršič A, Jagličić Z, Lisjak D (2010) The concept of low-temperature synthesis for superparamagnetic $BaFe_{12}O_{19}$ particles. J Am Ceram Soc 93:1602–1607

Ferk G, Krajnc P, Hamler A, Mertelj A, Cebollada F, Drofenik M, Lisjak D (2015) Nanocomposites of barium hexaferrite platelets in PMMA. Sci Rep 5:11395

Fuerdi-Milhofer H (1981) Spontaneous precipitation from electrolytic solutions. Pure Appl Chem 53:2041–2055

Jenuš P, Lisjak D (2014) The influence of material properties on the assembly of ferrite nanoparticles into 3D structures. Mater Chem Phys 148:1131–1138

Jolivet JP (2000) Metal oxide chemistry and synthesis. Wiley, Chichester

Kodama RH (1999) Magnetic nanoparticles. J Magn Magn Mater 200:359–372

Lee SW, Drwiega J, Mazyck D, Wu CY, Sigmund WM (2006) Synthesis and characterization of hard magnetic composite photocatalyst-barium ferrite/silica/titania. Mater Chem Phys 96:483–488

Li CX, Yang J, Yang PP, Lian HZ, Lin J (2008) Hydrothermal synthesis of lanthanide fluorides LnF_3 (Ln = La to Lu) nano-/microcrystals with multiform structures and morphologies. Chem Mater 20:4317–4326

Lisjak D, Drofenik M (2012) Chemical substitution—an alternative strategy for controlling the particle size of barium ferrite. Cryst Growth Des 12:5174–5179

Lisjak D, Ovtar S, Kovač J, Gregoratti L, Aleman B, Amati M, Fanetti M, Makovec D (2014) A surface-chemistry study of barium ferrite nanoplates with DBSa-modified surfaces. Appl Surf Sci 35:366–374

Makovec D, Kodre A, Arčon I, Drofenik M (2011) The structure of compositionally constrained zinc-ferrite spinel nanoparticles. J Nanopart Res 13:1781–1790

Makovec D, Primc D, Šturm S, Kodre A, Hanžel D, Drofenik M (2012) Structural properties of ultrafine Ba-hexaferrite nanoparticles. J Solid State Chem 196:63–71

Matijević E (1987) Uniform colloidal barium ferrite particles. J Colloid Interface Sci 117:593–595

Mertelj A, Lisjak D, Drofenik M, Čopič M (2013) Ferromagnetism in suspensions of magnetic platelets in liquid crystals. Nature 504:237–241

Mitsumata T, Wakabayashi T, Okazaki T (2008) Particle dispersibility and giant reduction in dynamic modulus of magnetic gels containing barium ferrite and iron oxide particles. J Phys Chem B 112:14132–14139

Moon SY, Sekino T, Kusunose T, Tanaka SI (2009) Simple one-step synthesis of water and organic media soluble gold nanoparticles with various shapes and sizes. J Cryst Growth 311:651–656

Pawley G (1981) Unit-cell refinement from powder diffraction scans. J Appl Crystallogr 14:357–361

Primc D, Makovec D, Lisjak D, Drofenik M (2009) Hydrothermal synthesis of ultrafine barium hexaferrite nanoparticles and the preparation of their stable suspensions. Nanotechnology 20:31605

Pullar RC (2012) Hexagonal ferrites: a review of the synthesis, properties and applications of hexaferrite ceramics. Prog Mater Sci 57:1191–1334

Röschmann P, Lemke M, Tolksdorf W, Welz F (1984) Anisotropy fields and FMR linewidth in single-crystal Al, Ga, Sc substituted hexagonal ferrites with M structure. Mater Res Bull 9:385–392

Sada E, Kumazawa H, Cho HM (1991) Synthesis of barium ferrite ultrafine particles by a hydrothermal method. Ind Eng Chem Res 30:1319–1323

Srnivas A, Gopalan R, Chandrasekharan V (2009) Room temperature multiferroism and magnetoelectric coupling in $BaTiO_3$–$BaFe_{12}O_{19}$ system. Solid State Commun 149:367–370

Tian ZR, Voight JA, Liu J, McKenzie B, McDermott MJ, Rodriguez MA, Konishi H, Xu H (2003) Complex and oriented ZnO nanostructures. Nat Mater 2:821–826

Wang ML, Shih ZW (1991) Reaction mechanism of producing barium hexaferrite from γ-Fe_2O_3 and $Ba(OH)_2$ by hydrothermal method. J Cryst Growth 114:435–445

Wang F, Han Y, Lim CS, Lu Y, Wang J, Xu J, Chen H, Zhang C, Hing M, Liu X (2010) Simultaneous phase and size control of upconversion nanocrystals through lanthanide doping. Nature 463:1061–1065